universe

MDPI

Article

Physical Properties of Radio Stars Based on LAMOST Spectral Survey

Liyun Zhang [1,*], Yao Cheng [1], Xianming L. Han [1,2], Qingfeng Pi [3], Prabhakar Misra [4], Baoda Li [1] and Zhongzhong Zhu [1]

[1] Department of Physics and Astronomy, College of Physics, Guizhou University, Guiyang 550025, China; chengyao@stu.xmu.edu.cn (Y.C.); xhan@butler.edu (X.L.H.); gs.bdli21@gzu.edu.cn (B.L.); zzzhu@gzu.edu.cn (Z.Z.)
[2] Department of Physics and Astronomy, Butler University, Indianapolis, IN 46208, USA
[3] School of Pharmacy, Guizhou University of Traditional Chinese Medicine, Guiyang 550025, China; piqingfeng@126.com
[4] Department of Physics & Astronomy, Howard University, Washington, DC 20059, USA; pmisra@howard.edu
* Correspondence: liy_zhang@hotmail.com

Abstract: Radio emission has been detected for all types of stars in the Hertzsprung Russell diagram. Large Sky Area Multi-Object Fiber Spectroscopic Telescope (LAMOST) low and medium-resolution spectroscopic surveys provide a good opportunity to obtain the spectroscopic properties of radio stars. We cross-matched big data from the LAMOST DR7 low resolution spectral survey with a catalogue of radio stars, and obtained 449 stellar spectra of 258 stars. We detected 185 spectra with Hα emission. There are a total of 108 objects with repeated low resolution spectral observations, of which 63 show variations in the Hα line over a long time, about several months. We cross-matched LAMOST DR7 medium resolution spectra with the radio star catalogue. We obtained 1319 LAMOST medium-resolution spectra of the 156 radio stars and then calculated their equivalent widths (*EWs*) of the Hα line. Among them, 93 radio stars with Hα emission were found from the LAMOST medium resolution spectra, and 63 objects showed short and long-term variabilities, especially on a short time scale of approximately 20 min. Finally, we estimated the minimal detectable radio flux of the FAST telescope and provided a scientific plan for studying radio stars.

Keywords: stars; stellar activity; radio stars; spectroscopic; chromosphere

Citation: Zhang, L.; Cheng, Y.; Han, X.L.; Pi, Q.; Misra, P.; Li, B.; Zhu, Z. Physical Properties of Radio Stars Based on LAMOST Spectral Survey. *Universe* **2022**, *8*, 384. https://doi.org/10.3390/universe8070384

Academic Editor: John Martin

Received: 31 May 2022
Accepted: 6 July 2022
Published: 19 July 2022

1. Introduction

Radio waves have been detected in all types of stars across the Hertzsprung–Russell (HR) diagram [1,2]. Radio stars are defined as stars with continuum radiation at the radio wavelength. Radio emission has been detected from the accretion disks of young stellar objects [3], star–planet interactions between host stars with extra-solar planets [4], magnetic activity in T Tau stars [5], ultracool dwarfs [6], low-mass [7] and RS CVn stars [8], and binary interactions in eclipsing binary systems [9]. Thermal or non-thermal physical processes explain such detection. The most direct probes of physical non-thermal processes are stellar magnetic field activities or shock, wind–wind interaction, jets, stellar pulsation, particle acceleration, and energy release on stars. Thermal radio emissions include mass transport, stellar wind outflows, and circumstellar disk emission [2]. Bai et al. (2012) [10] used a 25 m radio telescope in Urumqi, China and made continuum and polarization observations on two RS CVn binaries, V772 Her and Beta Per. They detected two radio flares and determined their polarization fractions. The detection of radio emissions from nearby stars is one of the earlier scientific projects of the Five-Hundred-Meter Aperture Spherical Radio Telescope (FAST) [11,12]. Observations of radio stars can both enrich our understanding of their physical parameters and active phenomena and promote the development of stellar theory in the radio domain with cm wavelengths.

Wendker [13,14] released an updated catalogue of 3699 single radio stars and binary systems. The Large Sky Area Multi-Object Fiber Spectroscopic Telescope (LAMOST) has recently offered stellar parameters from low and medium-resolution spectra [15–17], which are extremely useful for studying the chromospheric activity of solar-like stars and other chromospheric active stars in the Hα and Ca II IRT lines [18–22]. Zhang et al. (2017) [23] analyzed 147 spectra of 89 active radio stars in the catalogue of radio stars using the LAMOST low resolution survey DR2. They found that 28 stars exhibited long-term variation of chromospheric activity among 36 objects. Gizis et al. (2002) [24] and Lee et al. (2010) [25] found that approximately 30% of low mass stars showed variations in the Hα emission in short time scales of minutes to hours. In this study, we determined the nature of the physical parameters and optical properties of radio stars using LAMOST, particularly the time series of medium-resolution spectra. The relationship between the optical and radio wavelengths of nearby radio stars should be determined in the future.

The remainder of this paper is organized as follows. Based on the LAMOST low and medium resolution spectral surveys, we provide updated parameters of radio stars in Section 2. Then, we analyze the spectroscopic properties and variations in the Hα line in Section 3. Finally, we discuss the variation in the Hα line and provide an observational plan of the FAST telescope in Section 4.

2. Data

LAMOST is a reflecting Schmidt optical telescope with an effective aperture of 4 m and a field view of approximately 5 square degrees which is operated by the National Astronomical Observatories of China (NAOC); it is designed for low- and medium-resolution spectroscopic surveys [26,27]. In 2018, it was used to obtain a time series of the medium-resolution spectral survey [28]. More than 9.16 million LAMOST stellar spectra with a signal-to-noise ratios (SNR) above 10, and 6.20 million stellar parameters, were published on 30 June 2019 from the low resolution LAMOST DR7 [15,17]. There are two observational modes for the surveys of the LAMOST medium resolution spectra, namely, non-time domain and time-domain modes. A total of 0.67 million spectra of 0.51 million stars with an SNR of above 10 have been reported, and 0.51 million stellar parameters have been published as non time-domain data under the medium resolution. In addition, there are 1.61 million spectra of 0.29 million objects with SNR above 10. In total, 2.28 million spectra with an SNR above 10 and 0.81 million stellar parameters have been published. A standard reduction process was used to obtain the stellar parameters (e.g., the effective temperature, surface gravity, and metallicity) [15,29].

The LAMOST low- and medium-resolution spectra provide useful information for studying the chromospheric activity and parameters of radio stars. We cross-matched the LAMOST DR7 catalogue with the radio stars which were detected at least once and those with upper limits [13,14]. We obtained 449 stellar spectra of 258 radio stars with an SNR greater than about 10. We have listed the parameters of all the spectra of the radio stars in Table 1 and the repeated observations in Table 2. We have listed the LAMOST name (first column), number of radio stars (second column), other names (third column), observational HJD date (fourth column), exposure time (fifth column), spectral type (sixth column), and SNR using an R filter (seventh column). In addition, we cross-matched the radio stars with the medium spectra of LAMOST DR7. We obtained 1319 stellar spectra of 156 radio stars with an SNR above 10. In Table 3, we have listed the LAMOST name (first column), radio star number (second column), other names (third column), HJD (fourth column), exposure time (fifth column), and SNR (sixth column). We have listed only those parameters important for radio stars.

Table 1. Parameters of radio stars observed in LAMOST low resolution spectral survey along with their Hα properties.

LAMOST Name	Radio No.	Other Name	HJD	Exposure	Sp	SNR	Hα	Hα Height	Emission	Hβ	4.8 GHz	23 GHz	Mechanism
-	-	-	d	s	-	-	Å			Å	mjy	mjy	
J035721.13+125815.7	476	RX J0357.3+1258	58522.80069	1800	F9	261	-0.712 ± 0.015	5	a	-1.404 ± 0.040	-	-	disk
J040519.59+200928.1	508	RX J0405.3+2009	57437.78403	1800	G9	576	-0.329 ± 0.003	8	a	-0.888 ± 0.032	<0.8	-	disk
J040540.36+224812.0	512	DM +22 630	57397.92222	1800	-	8	-1.802 ± 0.265	3	a	-0.736 ± 0.156	-	-	disk
J040651.35+254128.2	523D	RX J0406.8+2541	56972.06944	1800	M0	346	4.674 ± 0.346	8	e	2.785 ± 0.117	-	-	disk
J040909.90+290130.2	539	RX J0409.1+2901	56967.09722	1800	G8	539	-0.015 ± 0.001	2	a	-0.678 ± 0.024	<0.29	-	disk
J041327.22+281624.6	566D	HBC 366	56967.09722	1800	M0	328	1.936 ± 0.058	10	e	1.440 ± 0.041	4.82	<14	disk
J041412.87+281209.9	570D	HD 283447	56967.09722	1800	K4	793	1.504 ± 0.047	5	e	0.651 ± 0.025	3.8–29	24–42	binary
J041430.60+285129.8	575	LkCa 2	56682.81875	1800	M0	90	1.677 ± 0.020	23	e	1.893 ± 0.122	<0.65	<12	disk
J041447.98+275234.6	581	HBC 368	56967.09722	1800	M2	556	2.057 ± 0.052	12	e	1.770 ± 0.062	<0.6	<14	disk
J041551.37+310035.7	589	RX J0415.8+3100	56981.05417	1800	G3	234	-0.830 ± 0.015	7	a	-1.592 ± 0.047	<0.20	-	disk
J041926.27+282613.9	654D	V819 Tau	56682.78125	1800	K7	142	2.856 ± 0.068	23	e	1.622 ± 0.054	<0.24	34.	magnetic
J041929.78+214513.9	659	LP 358-685	57397.92222	1800	M3	237	4.381 ± 0.106	42	e	6.516 ± 0.331	<0.5	-	disk
042049.82+300915.5	668	RX J0420.8+3009	56682.81875	1800	M0	54	1.821 ± 0.065	8	e	1.083 ± 0.104	-	-	disk
J042155.63+275506.0	681D	DE Tau	56682.78125	1800	M1	142	24.035 ± 10.453	5	e	38.107 ± 1.336	<0.58	36.	disk
J042158.91+281803.2	683D	DM +27 657	57377.95625	1800	G4	482	-0.295 ± 0.004	9	a	-1.309 ± 0.043	0.33–3.29	<15	disk
J042203.15+282538.7	686	HBC 382	56682.81875	1800	M1	177	4.021 ± 0.166	15	e	3.089 ± 0.139	<0.65	<12	disk
J042159.64+193207.2	688D	T Tau	57409.86389	1800	K3	408	-6.043 ± 6.214	0	a	19.578 ± 0.899	-	-	disk
...	...	...	...	...	...	...	...	...	...	...	...	...	

We only listed the radio intensities of 4.8 and 23 GHz with the most radio observations. For many stars there are no flux values at 4.8 and 23 GHz, as their intensities are at 1.4, 8.6 GHz, or other radio wavelengths. All of the radio intensities of radio stars in all of the radio wavelengths can be downloaded from the internet (https://cdsarc.cds.unistra.fr/viz-bin/cat/VIII/99 (accessed on 30 May 2022)) [13,14].

Table 2. Radio stars with repeated spectra from low resolution LAMOST survey DR7 and their Hα variation in long time scales (several months).

LAMOST Name	Radio No.	Other Name	HJD	Exposure Time	Sp	SNR	Hα	Hα Height	Emission	Long Variation	Hβ	4.8 GHz	23 GHz
-	-	-	d	s	-	-	Å				Å	mjy	mjy
J042929.70+261652.8	891	FW Tau	56625.94028	3000	M6	79	10.915 ± 0.772	29	e	60v	10.725 ± 1.724	-	<15
J042929.71+261653.2	891	FW Tau	56284.95625	1200	M6	33	8.945 ± 0.712	18	e	60v	5.373 ± 0.791	-	<15
J043001.13+351724.7	901D	HBC 390	56570.15625	1800	M1	85	6.583 ± 0.522	12	e	61v	1.791 ± 0.178	0.5	<15
J043001.13+351724.7	901D	HBC 390	56325.8125	1200	A2V	17	7.942 ± 0.754	14	e	61v	-1.042 ± 0.075	0.5	<15
J043019.15+351745.4	908D	HBC 391	56570.15625	1800	G5	336	0.519 ± 0.012	2	e	62v	-1.151 ± 0.035	4.2	<18
J043016.55+243928.5	915	V587 Tau	57377.95625	1800	G2	81	-1.412 ± 0.064	8	a	63n	-1.839 ± 0.094	-	<20
J043016.54+243928.5	915	V587 Tau	56284.92778	1200	G2	37	-1.399 ± 0.045	8	a	63n	-1.914 ± 0.072	-	<20
J043029.61+242645.0	917D	FX Tau	57425.77292	1800	M1	268	7.538 ± 1.511	4	e	64v	4.505 ± 0.165	-	20.
J043029.61+242644.9	917D	FX Tau	56284.95625	1200	M1	111	5.482 ± 0.533	7	e	64v	2.655 ± 0.124	-	20
J043029.61+242644.9	917D	FX Tau	56284.92778	1200	M1	100	5.768 ± 0.580	7	e	64v	2.520 ± 0.116	-	20
J043051.38+244222.1	926	ZZ Tau	56284.95625	1200	M3	49	5.989 ± 0.453	12	e	65v	14.064 ± 3.309	-	<20
J043051.38+244222.1	926	ZZ Tau	56284.92778	1200	M3	43	6.535 ± 0.459	14	e	65v	11.374 ± 1.381	-	<20
J043123.81+241052.7	937	V927 Tau	56284.92778	1200	M4	68	4.540 ± 0.340	9	e	66v	4.722 ± 0.519	-	<20
J043123.81+241052.7	937	V927 Tau	56284.95625	1200	M4	79	4.159 ± 0.263	9	e	66v	3.783 ± 0.423	-	<20
J043123.81+241052.9	937	V927 Tau	58512.84167	1800	M4	31	6.208 ± 0.514	11	e	66v	5.119 ± 1.486	-	<20
J043130.42+203537.9	941	RX J0431.4+2035	56608.0125	3000	M2	210	4.534 ± 0.279	11	e	67v	13.380 ± 0.584	-	-
J043130.42+203537.9	941	RX J0431.4+2035	57060.77083	4500	M2	210	3.556 ± 0.217	8	e	67v	9.458 ± 0.561	-	-
J043150.56+242418.0	952D	HK Tau	56284.92778	1200	M2	34	13.623 ± 3.433	6	e	68v	11.754 ± 1.164	1.40	41–110
J043150.57+242417.3	952D	HK Tau	56239.10903	1800	M1	51	18.194 ± 6.180	6	e	68v	20.532 ± 2.073	<0.6	-
J043150.56+242418.0	952D	HK Tau	56284.95625	1200	M1	40	14.022 ± 3.530	6	e	68v	16.709 ± 2.458	1.40	41–110
J043150.57+242417.7	952D	HK Tau	58487.85903	4500	M2	194	13.960 ± 3.417	7	e	68v	9.764 ± 0.387	<0.6	<11
J043157.80+182136.2	959D	V710 Tau	56332.79236	1200	M1	67	19.860 ± 5.904	9	e	69v	13.506 ± 1.059	<0.6	60–71
J043157.79+182137.9	959D	V710 Tau	57437.83264	1800	M1	247	17.614 ± 4.873	7	e	69v	13.950 ± 0.458	<0.6	60–71
J043215.40+242859.7	962D	V806 Tau	58512.84167	1800	EM	46	15.250 ± 6.165	4	e	70v	18.243 ± 9.525	-	124
...	...	...	...	...	...	...	...	...	...	...	...	...	...

We list several parameters of radio stars with repeated observations. All parameters are available in the online journal.

Table 3. Radio stars with LAMOST medium-resolution spectra and their Hα variations in short time scale (about 20 min).

LAMOST Name	Radio No.	Other Name	HJD	Exposure Time	SNR	Hα	Emission	Short Variation	Mechanism
-	-	-	d	s	-	Å			
J042929.70+261652.7	891	FW Tau	58466.9125	1200	36	16.891 ± 0.189	y	y	disk
J042929.70+261652.7	891	FW Tau	58467.02639	1200	36	16.939 ± 0.125	y	y	disk
J042929.70+261652.7	891	FW Tau	58467.01042	1200	36	18.176 ± 0.167	y	y	disk
J042929.70+261652.7	891	FW Tau	58466.92917	1200	36	17.299 ± 0.090	y	y	disk
J042929.70+261652.7	891	FW Tau	58466.94514	1200	36	17.308 ± 0.184	y	y	disk
J042929.70+261652.7	891	FW Tau	58466.99375	1200	36	17.108 ± 0.191	y	y	disk
J042929.70+261652.7	891	FW Tau	58466.97778	1200	36	16.720 ± 0.149	y	y	disk
J042929.70+261652.7	891	FW Tau	58466.96111	1200	36	17.030 ± 0.233	y	y	disk
J042941.56+263258.2	895D	DH Tau	58143.79306	1200	44	36.716 ± 0.754	y	y	disk
J042941.56+263258.2	895D	DH Tau	58143.80972	1200	44	35.127 ± 0.719	y	y	disk
J042941.56+263258.2	895D	DH Tau	58143.82569	1200	44	34.032 ± 0.683	y	y	disk
J043049.21+211410.1	927	RX J0430.8+2113	58416.07014	1200	799	−0.530 ± 0.134	n	n	disk
J043049.21+211410.1	927	RX J0430.8+2113	58502.83611	1200	327	−0.747 ± 0.113	n	n	disk
J043049.21+211410.1	927	RX J0430.8+2113	58416.05417	1200	799	−0.664 ± 0.105	n	n	disk
J043049.21+211410.1	927	RX J0430.8+2113	58502.87222	1200	327	−0.890 ± 0.138	n	n	disk
J043049.21+211410.1	927	RX J0430.8+2113	58502.88889	1200	327	−0.859 ± 0.117	n	n	disk
J043049.21+211410.1	927	RX J0430.8+2113	58502.85625	1200	327	−0.783 ± 0.109	n	n	disk
J043049.21+211410.1	927	RX J0430.8+2113	58416.08681	1200	799	−0.649 ± 0.108	n	n	disk
J043049.21+211410.1	927	RX J0430.8+2113	58416.10278	1200	799	−0.668 ± 0.106	n	n	disk
J043049.21+211410.1	927	RX J0430.8+2113	58416.11875	1200	799	−0.562 ± 0.137	n	n	disk
J043049.21+211410.1	927	RX J0430.8+2113	58416.13542	1200	799	−0.531 ± 0.136	n	n	disk
J043049.21+211410.1	927	RX J0430.8+2113	58416.15139	1200	799	−0.527 ± 0.135	n	n	disk
J043049.21+211410.1	927	RX J0430.8+2113	58416.16736	1200	799	−0.530 ± 0.141	n	n	disk
J034548.28+322411.8	402D	HBC 20	58417.11319	1200	344	11.558 ± 0.0512	y	n	disk
J034548.28+322411.8	402D	HBC 20	58417.03194	1200	344	11.686 ± 0.0522	y	n	disk
J034548.28+322411.8	402D	HBC 20	58417.04861	1200	344	11.693 ± 0.0525	y	n	disk
J034548.28+322411.8	402D	HBC 20	58417.06458	1200	344	11.683 ± 0.0534	y	n	disk
J034548.28+322411.8	402D	HBC 20	58417.08056	1200	344	11.665 ± 0.0521	y	n	disk
J034548.28+322411.8	402D	HBC 20	58417.09722	1200	344	11.569 ± 0.0517	y	n	disk
J034548.28+322411.8	402D	HBC 20	58417.12917	1200	344	11.506 ± 0.0496	y	n	disk
...	...	...	...	...	...	...	...	...	...

There may be multiple mechanisms for Hα line on radio stars, which are from the published paper [13,14] and our data. The cause of the Hα emission can not be ascertained, and needs more data prior to confirmation. Here, we list several parameters of radio stars. All parameters are available in the online journal.

3. Spectroscopic Analyses

3.1. LAMOST Low-Resolution Spectroscopic Analyses

For the LAMOST low resolution spectra, we obtained the continuum using the two sides of different chromospheric active indicators based on the Hammer program, which was published in 2007 [30,31]. The regions of these two sides of these indicators are listed in previously published papers [31,32]. We used a similar method to reduce the spectra from the LAMOST survey [15]. This method has previously been used to reduce the SDSS spectra by other astronomers [33]. The published LAMOST radial velocity was used to revise the spectrum and determine the position of the Hα line. We calculated the equivalent widths (EWs) in the Hα, Hβ, Hγ, Hδ, and Ca II H&K and IRT lines using the integration method within the region of $\pm$10 Å around the core of the spectral lines. Simultaneously, we used the Gaussian function to fit the Hα line and obtained the Hα EW. The EW difference between the two methods is the uncertainty of the Hα EW. We listed the EWs (eighth column) and heights (ninth column) of Hα. Using the EWs of the Hα indicator, we determined the behavior of the absorption or emission (10th column). For the OBAFGK stars, we used the criterion of EW 0 Å. If the EW value of the Hα line was above 0 Å and simultaneously larger than the errors and the value of the height of the Hα line was three times larger than the standard error [34], we considered the behavior of the Hα line to be emission. However, the EW must be larger than 0.75 Å, because there are numerous molecular lines for M-type stars [23,31]. We have listed the EW of Hβ in the 11th column of Table 1 and the radio intensities at 4.8 GHz and 23 GHz in the 12th and 13th columns of Table 1. The printed versions of the tables include other values of all active chromospheric active indicators, and will be made available in the online database at the CDS. Among the 150 radio stars with single spectra, 77 radio stars had emissions. Several examples of radio stars with single spectra are plotted in the left-hand panels in Figure 1. There are obvious emissions of the Hα, Hβ, Hγ, Hδ, H8, Ca II H&K and IRT lines. In addition, there are 299 spectra of 108 objects with repeated observations of radio stars. Similar to Table 1, we list the parameters of the radio stars with repeated spectra in Table 2. The amplitude of the Hα EW variability is three times larger than the error, and we considered the radio star as a variable [23]. Among them, 69 objects show a long time variation in their Hα intensity. We plotted two examples and marked different chromospheric activity indicators in the right panels of Figure 1. In the small window of the right panel, the details of the Hα variation are clearly presented.

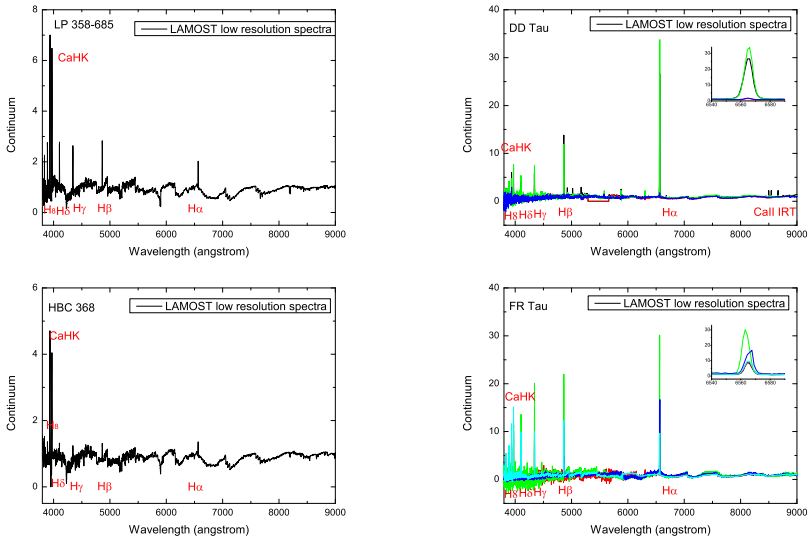

Figure 1. Examples of the low resolution LAMOST spectra of several radio stars with single (**left**) and repeated (**right**) observations. We marked several important spectral lines with obvious emissions in the Ca II H&K, Hδ, Hγ, Hβ, Hα, and Ca II IRT lines. There are obvious variations in the Hα line in the small panels.

3.2. LAMOST Medium-Resolution Spectroscopic Analyses

For the total coadd spectra from LAMOST medium-resolution spectra, cosmic rays have been reduced. To discuss the variation in the Hα line of the radio star on a short time scale of approximately 20 min, we used the single exposure spectra. However, there are cosmic rays in these single spectra of the DR7 released data of the LAMOST. First, we needed to detect and remove the cosmic rays from the single exposure spectra. We calculated the ratio of the data above the mean of the surrounding wavelengths. If there were typical values five times or higher than the standard deviation of the background, we considered the points as cosmic rays and removed them for numerous runs. The detected cosmic rays were replaced by the average value of the neighboring pixels. Multiple detection passes are required to detect and replace cosmic ray events. As there are many repeated observations for LAMOST medium spectra, we reduced the cosmic rays using the cross-judgement method. In Figure 2, we provide several examples of the observed medium-resolution LAMOST spectra with cosmic rays (left) and the results of our reduction with no cosmic rays (right). We obtained the continuum spectra of the radio stars by 5- or 6-order polynomial function fitting and normalised spectra after normalisation. We plotted the observed (right panel) and normalised (left panel) LAMOST spectra, as shown in Figure 3. The methods used for obtaining the *EW*s and their uncertainties were similar to those reported by Zhang et al. (2020) [21].

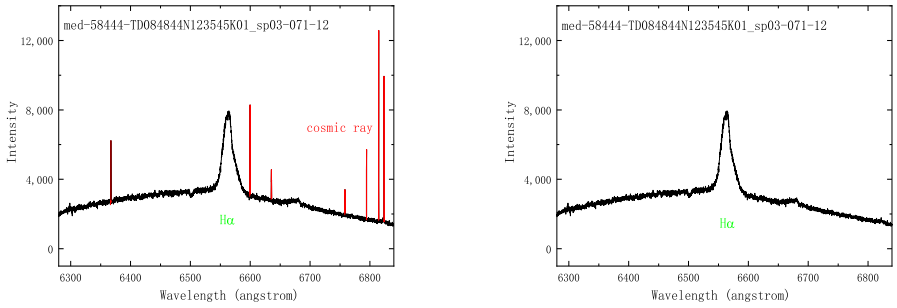

Figure 2. Observed medium-resolution LAMOST spectra with cosmic rays (**left**) and reduction spectra with no cosmic rays (**right**). The red lines are cosmic rays in the observed spectra.

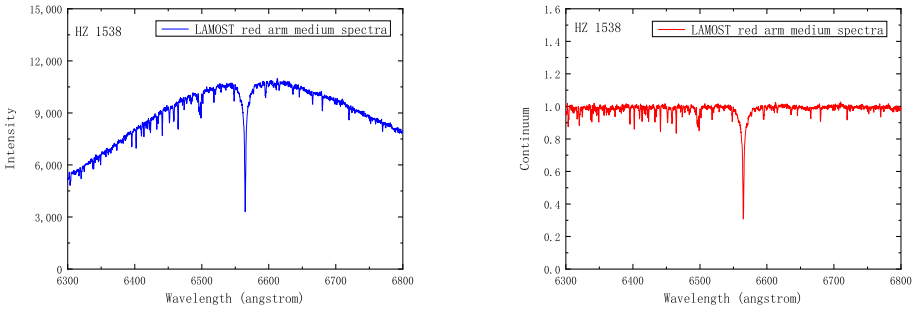

Figure 3. Observed medium-resolution LAMOST spectra (**left**) and its normalised spectrum (**right**).

3.3. Comparison between Low-Resolution and Medium-Resolution LAMOST Spectra

By cross-matching the LAMOST low- and medium-resolution catalogue of radio stars, we found 102 objects with both low and medium resolution spectroscopic observations. Figure 4 shows several examples of FP Tau, FX Tau, DL Tau, and DM +25 1065 with two spectral observational modes. In Figure 4, it can be seen that there is a single peak emission of the low-resolution spectra. However, there are two or more peaks in the medium-resolution spectra because of the higher resolution of 7500. These emissions are caused by the substructures of the stellar disk, different regions of the chromospheric active region, or

different components of binaries. Medium-resolution spectra are extremely important for investigating the details of spectroscopic binaries and special physical phenomena.

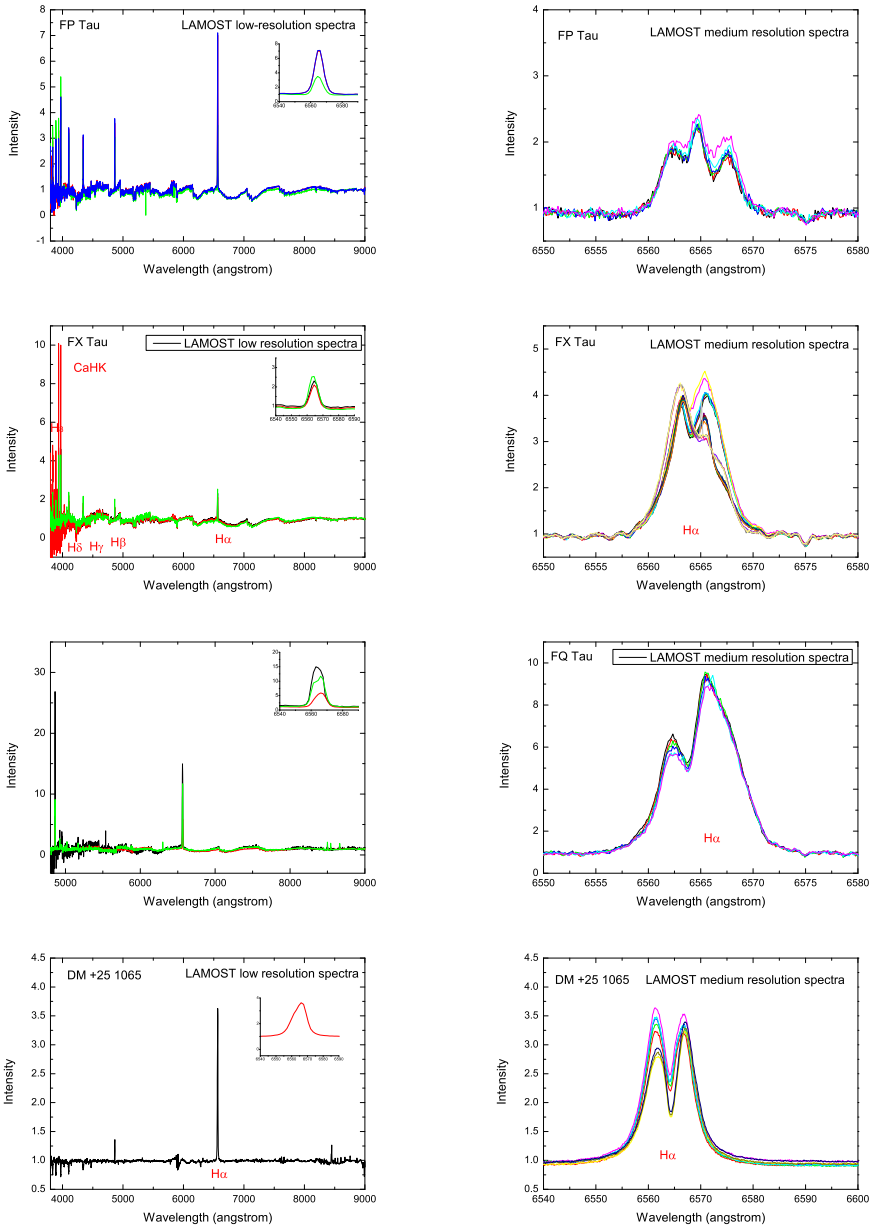

Figure 4. LAMOST spectra of radio stars with both low (**left**) and medium (**right**) resolution observations. We marked several important spectral lines with obvious emissions in the Ca II H&K, Hδ, Hγ, Hβ, Hα, and Ca II IRT lines. Detailed behavior of the Hα line is shown in the small panels. The right panel shows the detailed behavior of LAMOST medium-resolution spectra, and different colors represent the different observations.

3.4. Short-Term and Long-Term Scale Variations of the Hα Line

The time domain medium-resolution observations were made using the LAMOST telescope. These can be used to discuss the Hα variations of radio stars over short time scale of approximately 20 min. There are 1319 spectra of 156 objects with repeated observations. There are 93 objects with Hα emission. Among them, the emission intensities of 29 active objects are stable on a short time scale. We have plotted several examples (HBC 20, DK Tau, GO Tau and GG Tau) of radio stars with stable Hα emissions in Figure 5, where the continuum spectra are shown in the left panel and the Hα EW values are shown in the

right panel. The Hα emissions of 63 objects show short and long time scale variations, especially short time scale of approximately 20 min. It is interesting to note that there are short time variations of 20 min in CY Tau, BP Tau, Hubble 4, HBC 230, and V590 Mon. We have plotted examples of the LAMOST medium resolution spectra of radio stars in the left panel of Figure 6. The variation in the Hα EW is shown in the right panel of Figure 6. We can observe the increase and decay phases of the Hα variation. Similar to Figure 6, we show examples with obvious long-term variations in the EW of the Hα line in Figure 7. More data on the Hα intensity are required to detect the chromospheric activity cycle in the future.

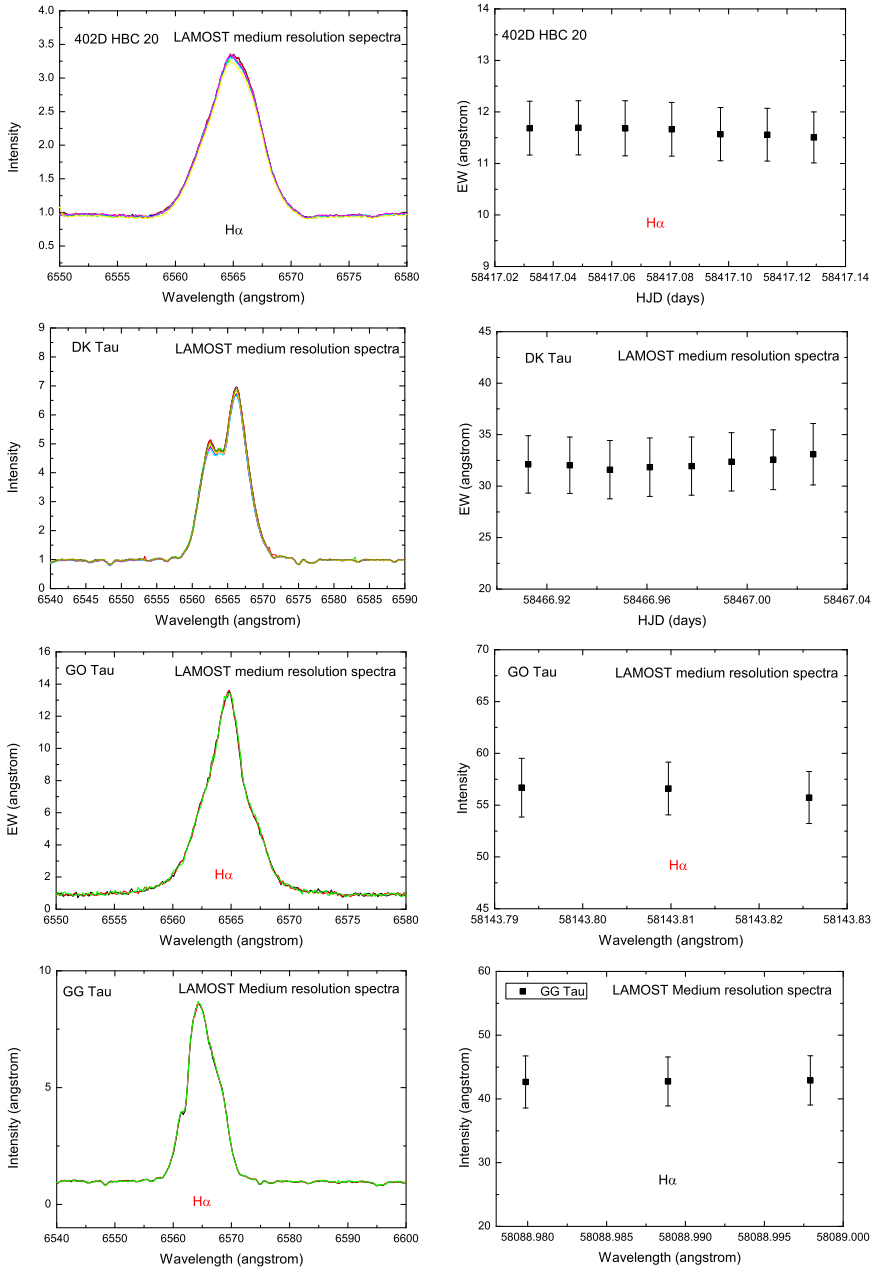

Figure 5. Examples of radio stars with stable Hα emissions and EWs.

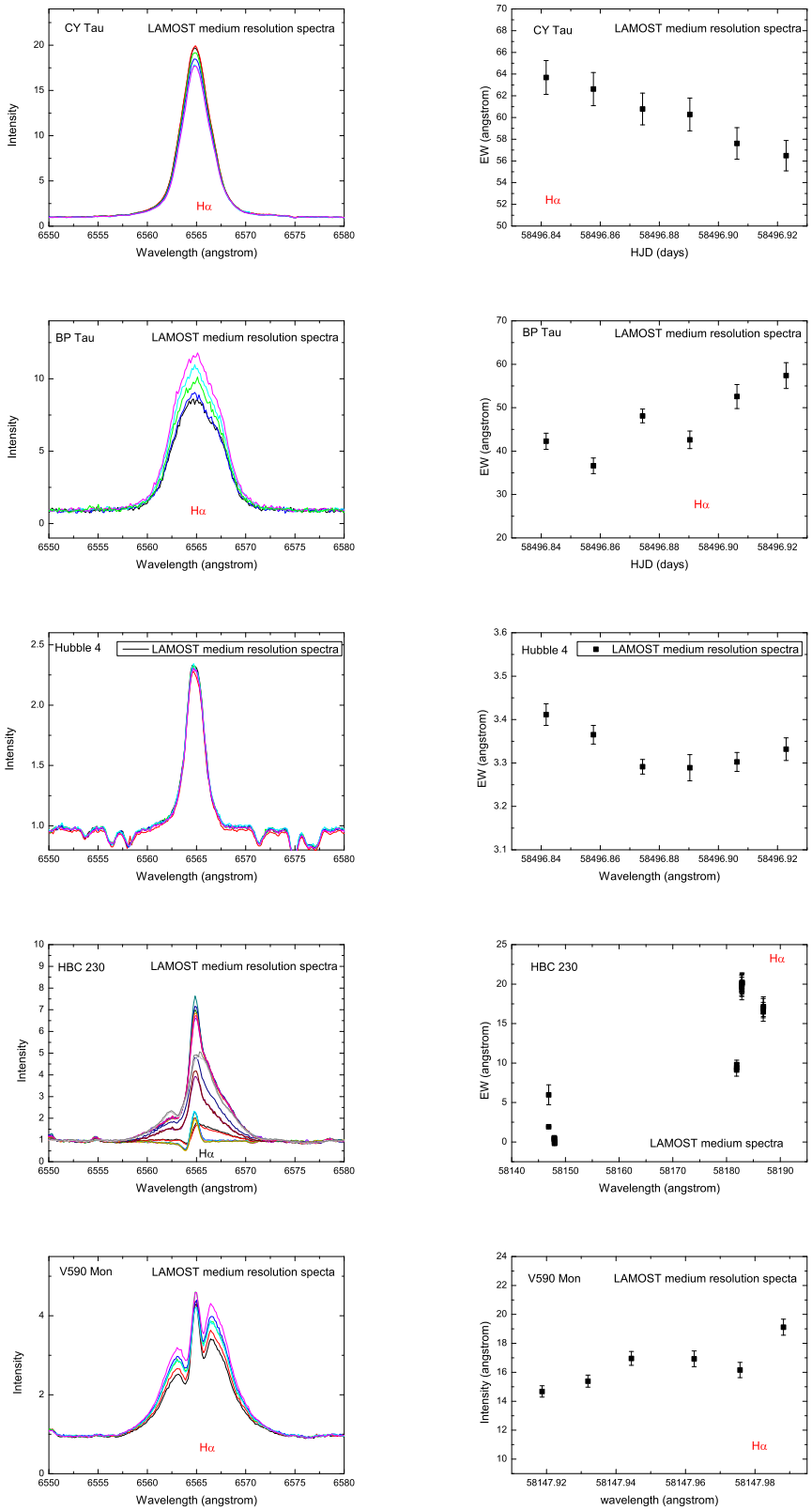

Figure 6. Medium resolution LAMOST spectra of radio stars with repeated observations on short time scale (**left**). The short-term variation of EW is shown on the (**right**).

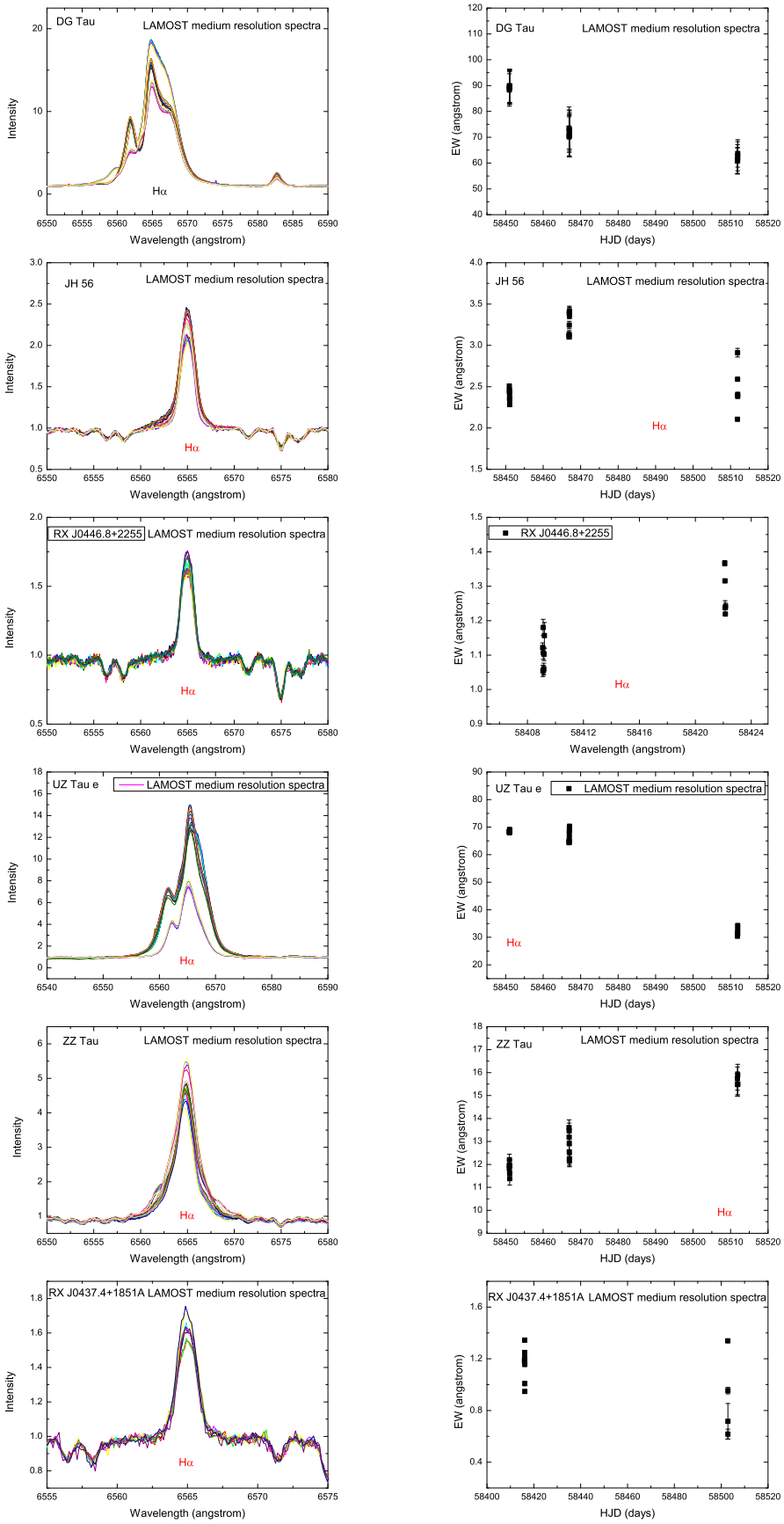

Figure 7. Medium resolution LAMOST spectra of radio stars with repeated observations over a long time scale of several months (**left**). There are obvious long-term variations in the EWs of Hα, as shown in the (**right**) panel.

4. Discussion and Conclusions

We have investigated the Hα behavior of the detected radio stars and discussed the properties of short and long-term variations. We have additionally considered the radio stars in the observational region of the FAST.

4.1. Behavior of the Hα Line and Variation

We detected 449 low-resolution spectra for 258 objects. There were 185 objects with emissions above the continuum of the Hα line. There were 108 objects with the repeated observations, with 63 objects exhibiting long-term variations. We additionally obtained 1319 LAMOST medium-resolution spectra of 156 radio stars. Comparing the low- and medium-resolution LAMOST spectra, the medium-resolution spectra show more detailed behaviour. There are 93 radio stars with medium-resolution spectra with Hα emissions. Among them, 63 objects exhibited short- and long-term variability, particularly at a short time scale of approximately 20 min. The properties of Hα emission and spectral line variation of the radio stars are due to different physical mechanisms, including photo-star disks, stellar activity, and binary systems. For our data, we have provided the possible mechanism in the last columns of Tables 1 and 3. The cause of the Hα emission cannot be ascertained in the present paper, as we need more data to confirm it.

Most of our objects are young stars (such as FP Tau, FW Tau, DH Tau, HBC 230, etcetera). For young objects, the Hα emission can be explained by strong stellar winds, circumstellar discs, and outflow activity [35–37]. For solar-like and cool dwarf stars (such as UX Com,...), the short and long-term variations are due to magnetic phenomena. The short term variations can be explained by chromospheric activity of plages or flares, prominence, post-flare loops, and other chromospheric activity phenomena [38]. Several of our objects are eclipsing binaries, such as AC Cnc, DM +16 516), in which case the variations are caused by the activity of the two components or their interactions [39]. The chromospheric variation might be explained by orbital phase modulation of chromospheric emission [39] or chromospheric activity longitudes [40]. Long-term chromospheric variation was found on RX J0437.4+1851A and JH 56, which was explained by stellar Hα activity evolution [41]. As data from the time series LAMOST medium-resolution survey accumulated, we were able to detect the chromospheric activity cycles. There is an obvious EW decrease for CY Tau and an EW increase for BP Tau in the short time scales in Figure 6. If the intensity of the Hα emission shows a rapid increase followed by a gradual decrease, the phenomenon might be due to a flare event [42]. We expect to search for flare events with rise and decay in the future.

There were numerous objects (FP Tau, FX Tau, FQ Tau, DM +25 1065,...) observed in the low and medium-resolution spectral surveys. The medium-resolution spectra are more detailed than the low resolution spectra. We can see self-absorption in the Hα emission of early stars in Figure 4, which might be caused by accretion and outflow regions of circumstellar discs [43]. While we were able to confirm that the disks were more complex [37], we need more spectral data on the complete orbital phases to determine the disk structure. Meng et al. (2021) [44] identified two emissions from the primary and secondary components of eclipsing binary 2MASS J04100497+2931023 using the LAMOST medium spectra. This binary with both blended emissions and double Hα emissions might be caused by the two components of the active binaries [45]. The medium LAMOST spectral survey only started a few years ago, and thus the data for each object are insufficient. Here, we provide the complex and detailed theoretical mechanism and discuss the relationship between the optical and radio radiation.

4.2. Observational Plan of Radio Stars Using FAST

Wendker [13,14] published an updated catalogue of 3699 radio stars or binary systems. Owing to its excellent radio detection capability, we anticipate using the FAST telescope to observe radio stars, especially the nearby radio stars, in the future. Our project is dedicated to revealing the nature of radio emissions. Based on the latitude coverage of the sky from

−14.6 to 65.6 Dec for FAST, we plotted the distribution of the radio stars in Figure 8, where the red points are within the observation region of FAST.

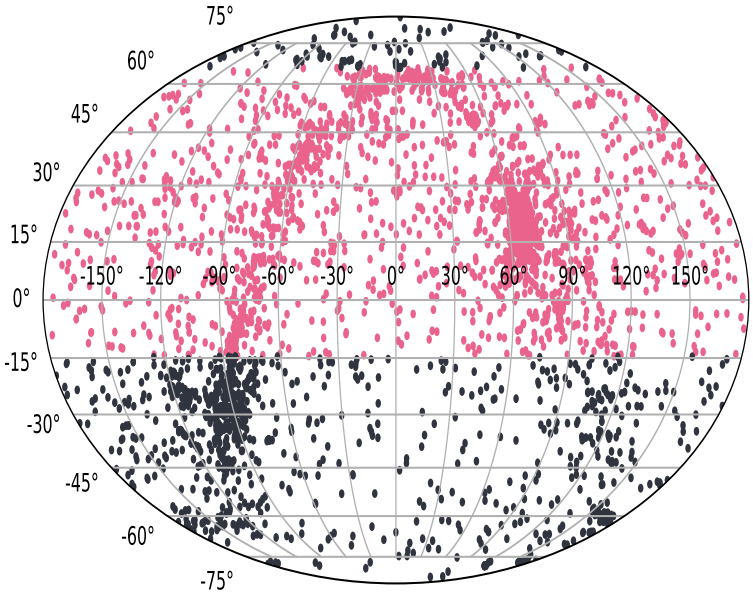

Figure 8. Position distribution of radio stars; red points are within the observational field of the FAST telescope.

The formula for the minimal detection flux density of the radio telescope is as follows:

$$S_{min} = \frac{2KT_{sys}}{\eta A\sqrt{\Delta\eta_p t}} \quad (1)$$

where K is the Boltzmann constant, K = 1.38 × 10^{-23} erg/k, T_{sys} is the telescope system temperature, T_{sys} = 27 k. η is the aperture efficiency of the telescope, η_{min} = 0.55. A is the effective aperture area of the radio telescope (the effective aperture area of FAST is 300 m in diameter), η_p is a fixed value, η_p = 2, Δ bandwidth is 500 MHz, t is the sampling time, and we take t = 1 s. Based on these parameters [46], we can estimate the minimal detectable radio flux (S_{min} ∼ 60 μJy) of the FAST telescope.

We compared the flux of radio stars at 1.4 GHz with the minimal radio observational flux of FAST. We show the observational ability of FAST in Figure 9, where the horizontal axis is the number of radio stars in descending order of declination and the vertical axis is the intensity of the radio stars. For data points, the magenta five-pointed stars represent the real value of the radio flux, the green circles represent the upper limit of the radio flux, and the red line represents our estimated limit of the radio flux of FAST. It can be seen that FAST can theoretically detect the flux for the samples of radio stars above the limited line. In addition, the detection frequency band of the FAST telescope is limited to [47] (70 MHz∼3 GHz), and the limitation of the observation sky is Dec: −14.5∼65.6. We were thus able to obtain samples from the yellow region, as shown in Figure 9. The horizontal axis represents the serial number according to the size of the declination of the radio stars. The red dots in Figure 9 are above the detection limit of FAST, and are thus easy to detect. For the green points, the maximum possible value of the radio stars is above the detection limit of FAST, and we thus need to use FAST to conduct further validation checks. We have listed these in Table 4, as they are likely to be detected by FAST.

Table 4. Radio stars expected to be observed by FAST in the 1.4 GHz band.

Star Name	S_v (mJy)	Ra	Dec	Star Name	S_v (mJy)	Ra	Dec
V 711 Tau	56	03 34 13.151	+00 25 33.09	RS CVn	0.8	13 08 17.891	+36 12 01.23
V 711 Tau	64	03 34 13.151	+00 25 33.09	BH CVn	4.02	13 32 33.923	+37 26 16.49
V 711 Tau	70	03 34 13.151	+00 25 33.09	BH CVn	9	13 32 33.923	+37 26 16.49
V 711 Tau	100	03 34 13.151	+00 25 33.09	XTE J2012+381	3.5	20 10 47.86	+38 01 56.5
V 711 Tau	135	03 34 13.151	+00 25 33.09	SAO 61224	1.67	09 00 17.091	+38 02 29.99
BI Cet	2.17	01 20 16.665	+00 27 15.98	12 ALF(2) CVn	0.85	12 53 40.181	+38 35 03.42
GSC	2.42	21 35 07.444	+01 23 42.26	BM CVn	1.06	13 19 17.318	+39 08 31.80
YZ CMi	1.32	07 42 03.870	+03 40 48.50	SAO 64090	7.1	14 19 02.311	+39 12 53.99
V 1343 Aql	650	19 09 21.282	+04 53 54.27	SAO 64090	9	14 19 02.311	+39 12 53.99
DM +00 198	<0.7	01 10 27.453	+00 48 52.39	HD 276968	<0.6	04 49 11.948	+43 13 43.30
EC 95	<6	18 27 25.5	+01 10 42.	HD 30650	<0.6	04 47 58.294	+43 29 39.34
YZ CMi	<140	07 42 03.870	+03 40 48.50	DM +43 3571	<1	20 18 46.720	+43 41 43.33
HD 219188	<0.6	23 11 27.893	+04 43 29.19	68 Cyg	<0.6	21 16 35.169	+43 44 05.51
47 RHO Leo	<0.6	10 30 10.762	+09 33 52.22	HD 4142	<0.6	00 41 38.936	+47 35 25.64
HD 39680	<0.6	05 51 54.528	+13 50 48.09	V 819 Cyg	<0.6	19 51 32.365	+47 40 36.45
HR 2222	<0.6	06 12 18.204	+13 52 03.46	HD 20218	<0.6	03 13 53.308	+47 56 47.84
T Tau	2.8	04 19 04.209	+19 25 05.67	V 1016 Cyg	17	19 55 19.835	+39 41 29.59
AD Leo	140	10 16 53.863	+20 07 19.20	MWC 349	68	20 30 56.836	+40 29 20.81
PS Ser	0.93	15 41 46.963	+22 29 48.17	Algol	100	03 04 54.343	+40 45 52.16
FK Com	1.75	13 28 24.780	+24 28 25.39	V 1521 Cyg	14,680	20 30 37.62	+40 47 12.85
DH Leo	1.08	09 57 13.283	+24 47 36.76	Cyg OB2-9	4.8	20 31 22.958	+41 04 50.39
MS Ser	2.26	15 56 38.067	+25 42 45.42	Tycho 3429 1609	1.8	09 37 54.550	+48 49 48.87
SAO 146194	2.26	15 56 38.067	+25 42 45.42	MWC 84	120	04 15 39.18	+55 52 46.1
V 340 Gem	6.5	07 18 28.136	+26 15 16.80	SAO 29070	1.31	14 14 22.905	+56 59 18.20
V 340 Gem	9.9	07 18 28.136	+26 15 16.80	54 Cam	1.02	07 58 32.107	+57 24 50.89
Gliese 171.2	1019	04 33 41.765	+27 02 01.03	NOV Mon 75	300	06 20 11.176	−00 19 10.80
17 SIG CrB	4.7	16 12 48.306	+33 59 02.91	HD 201910	<0.6	21 09 27.402	+40 58 47.05
17 SIG CrB	6.8	16 12 48.306	+33 59 02.91	HR 6146	<0.73	16 26 59.860	+41 59 26.35
53 Ari	<0.6	03 04 36.481	+17 41 18.52	DM +49 2596	<0.64	17 09 06.804	+49 01 35.37
HD 248434	<0.6	05 48 42.	+21 32	HD 216534	<0.6	22 50 47.943	+49 35 55.19
HD 214930	<0.6	22 39 02.017	+23 35 06.44	AM Her	<0.24	18 14 58.75	+49 50 54.9
RU Cnc	<0.64	08 34 33.729	+23 44 12.58	HD 14220	<0.6	02 16 14.755	+52 19 55.07
ST LMi	<0.64	11 02 58.0	+25 22 42	MWC 84	<2	04 15 39.18	+55 52 46.1
UX Ari	54	03 23 33.027	+28 32 32.43	NOV Mon 75	300	06 20 11.176	−00 19 10.80
UX Ari	63	03 23 33.027	+28 32 32.43	AZ Psc	1.28	22 56 18.789	−00 35 03.43
75 SIG Gem	3.6	07 40 11.390	+29 00 22.34	AY Cet	2.55	01 14 03.832	−02 45 46.70
HD 72146	6.5	08 29 13.865	+29 29 23.06	M 2-9	32	17 02 52.588	−10 04 31.16
LB 10117	5	11 16 24.07	+30 08 17.9	46 KSI Per	<0.6	03 55 42.806	+35 38 56.45
J1408+3054	3.3	14 05 53.56	+31 09 00.0	HD 37737	<0.6	05 39 08.716	+36 10 36.86
66 ALF Gem	0.76	07 31 24.725	+31 59 59.20	XTE J2012+381	<1	20 10 47.86	+38 01 56.5
Tycho 2553 316	1.07	14 24 34.273	+32 05 41.05	HD 192281	<0.6	20 10 46.724	+40 07 01.21

Table 4. *Cont.*

Star Name	S_v (mJy)	Ra	Dec	Star Name	S_v (mJy)	Ra	Dec
GJ 1108	5.9	08 05 45.95	+32 57 59.2	HR 1500	<0.6	04 40 44.928	+40 41 40.18
T CrB	<0.7	15 57 24.520	+26 03 38.70	22 LAM Cep	<0.6	22 09 48.513	+59 10 02.39
ZZ Boo	<0.67	13 53 51.821	+26 09 46.07	LSI +60 141	<0.6	01 04 53.3	+60 17 05.
Ross 868	<0.7	17 17 53.	+26 32 48.	SAO 20610	<0.6	23 22 18.396	+60 52 59.33
HD 39478	<0.6	05 41 00.576	+26 44 51.93	HD 16429	<0.6	02 36 53.641	+61 04 05.33
5 ALF CrB	<0.67	15 32 34.146	+26 52 54.42	DM -02 1885	<0.6	06 58 15.991	−03 02 43.49
WY Cnc	<0.67	08 58 58.0	+26 53 14.	DM -02 3312	<0.6	11 13 38.617	−03 11 56.90
Pollux	<0.67	07 42 15.512	+28 08 55.29	DM -05 4318	<0.6	16 31 47.917	−06 01 58.63
UX Com	<0.55	12 59 08.9	+28 54 02.	HD 125924	<0.6	14 20 03.717	−08 01 15.93
HD 195907	<0.6	20 31 03.680	+31 29 08.83	DM -08 4675	<0.6	18 38 04.177	−08 45 58.28
HD 201345	<0.6	21 05 51.711	+33 11 40.14	HD 220172	<0.6	23 19 15.073	−10 02 08.25
HR 1712	<0.6	05 12 59.774	+34 15 25.32	13 ZET Oph	<0.6	16 34 24.137	−10 28 02.81
GX 17+2	<0.2	18 13 10.920	−14 03 14.44	DM -10 4493	<0.6	17 23 30.808	−10 57 01.17
G 165-8	2.51	13 29 27.46	+29 32 02.4				

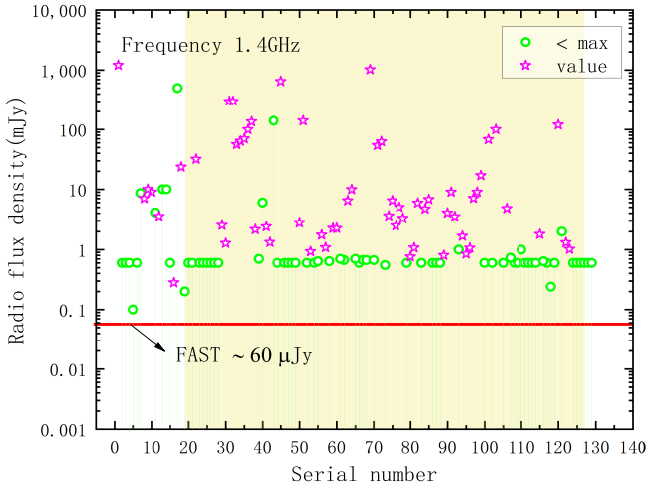

Figure 9. Distribution of the radio flux of radio stars in the 1.4 GHz frequency; the red line is the detection limit of the FAST telescope.

We have selected several interesting candidates from among the radio stars, such as the active stars from the LAMOST survey [21], ultracool dwarfs [48], and host stars with an extra-solar planet [49]. We intend to trace them over 4–6 h using FAST [28] and then attempt to detect their possible radio radiations. We might detect flare events and star–planet and binary interactions [9]. In the future the study of radio stars will be able to use both FAST and the upcoming SKA platform [50]. We intend to study non-thermal radio emission due to shock acceleration from the wind collision region of massive stars, the high energy emission process of young stellar objects [51,52], the generation and dissipation of kG-strength magnetic fields of ultra-cool dwarfs [53–55], and stellar and planetary magnetosphere interactions [56]. FIn the future, we will analyze the relationship between radio radiation and stellar physical parameters, as radio and optical emissions are required to determine the relationship between chromospheric and coronal emissions. The use of the FAST, SKA, and LAMOST platforms has the potential to unlock a great deal of new science concerning radio stars.

Author Contributions: Conceptualization, L.Z.; software, Y.C., B.L. and Z.Z.; investigation, Q.P.; writing—review and editing, L.Z., X.L.H. and P.M. All authors have read and agreed to the published version of the manuscript.

Funding: This research is funded by the Joint Fund of Astronomy of the NSFC and CAS Grant Nos. 11963002 and U1931132, and the China Manned Space Project, No. CMS-CSST-2021-B07. This research is also funded by the Cultivation Project for FAST Scientific Payoff Grant No. 2021.

Conflicts of Interest: The authors declare no conflict of interest.

References

1. Güdel, M. Stellar Radio Astronomy: Probing Stellar Atmospheres from Protostars to Giants. *Annu. Rev. Astron. Astrophys.* **2002**, *40*, 217–261. [CrossRef]
2. Matthews, L.D. Radio Stars: From kHz to THz. *Publ. Astron. Soc. Pac.* **2019**, *131*, 016001. [CrossRef]
3. Anglada, G.; Rodríguez, L.F.; Carrasco-González, C. Radio jets from young stellar objects. *Astron. Astrophys. Rev.* **2018**, *26*, 3. [CrossRef]
4. Trigilio, C.; Umana, G.; Cavallaro, F.; Agliozzo, C.; Leto, P.; Buemi, C.; Ingallinera, A.; Bufano, F.; Riggi, S. Detection of α Centauri at radio wavelengths: Chromospheric emission and search for star-planet interaction. *Mon. Not. R. Astron. Soc.* **2018**, *481*, 217–225. [CrossRef]
5. Aronow, R.A.; Herbst, W.; Hughes, A.M.; Wilner, D.J.; Winn, J.N. Optical and Radio Observations of the T Tauri Binary KH 15D (V582 Mon): Stellar Properties, Disk Mass Limit, and Discovery of a CO Outflow. *Astron. J.* **2018**, *155*, 47. [CrossRef]
6. Yu, S.; Hallinan, G.; Doyle, J.G.; MacKinnon, A.L.; Antonova, A.; Kuznetsov, A.; Golden, A.; Zhang, Z.H. Modelling the radio pulses of an ultracool dwarf. *Astron. Astrophys.* **2011**, *525*, A39. [CrossRef]

7. Llama, J.; Jardine, M.M.; Wood, K.; Hallinan, G.; Morin, J. Simulating Radio Emission from Low-mass Stars. *Astrophys. J.* **2018**, *854*, 7. [CrossRef]
8. Beasley, A.J.; Güdel, M. VLBA Imaging of Quiescent Radio Emission from UX Arietis. *Astrophys. J.* **2000**, *529*, 961–967. [CrossRef]
9. Peterson, W.M.; Mutel, R.L.; Güdel, M.; Goss, W.M. A large coronal loop in the Algol system. *Nature* **2010**, *463*, 207–209. [CrossRef]
10. Bai, J.Y.; Han, J.L.; Gao, X.Y.; Wang, C.; Zhang, L.Y. Polarization Observation Experiments for Radio Flares of Stars at 6 cm Band. *Acta Astron. Sin.* **2012**, *53*, 291–298.
11. Li, D.; Pan, Z. The Five-hundred-meter Aperture Spherical Radio Telescope Project. *Radio Sci.* **2016**, *51*, 1060–1064. [CrossRef]
12. Nan, R.; Li, D.; Jin, C.; Wang, Q.; Zhu, L.; Zhu, W.; Zhang, H.; Yue, Y.; Qian, L. The Five-Hundred Aperture Spherical Radio Telescope (fast) Project. *Int. J. Mod. Phys. D* **2011**, *20*, 989–1024. [CrossRef]
13. Wendker, H.J. Radio continuum emission from stars: A catalogue update. *Astron. Astrophys. Suppl. Ser.* **1995**, *109*, 177–179.
14. Wendker, H.J. *VizieR Online Data Catalog: Catalogue of Radio Stars (Wendker, 2001)*; Vizier Online Data Catalog; NASA: Washington, DC, USA, 2015; p. VIII/99.
15. Luo, A.L.; Zhao, Y.H.; Zhao, G.; Deng, L.C.; Liu, X.W.; Jing, Y.P.; Wang, G.; Zhang, H.T.; Shi, J.R.; Cui, X.Q.; et al. The first data release (DR1) of the LAMOST regular survey. *Res. Astron. Astrophys.* **2015**, *15*, 1095. [CrossRef]
16. Wang, R.; Luo, A.L.; Chen, J.J.; Bai, Z.R.; Chen, L.; Chen, X.F.; Dong, S.B.; Du, B.; Fu, J.N.; Han, Z.W.; et al. Properties of Radial Velocities Measurement Based on LAMOST-II Medium-resolution Spectroscopic Observations. *Astrophys. J. Suppl. Ser.* **2019**, *244*, 27. [CrossRef]
17. Wang, R.; Luo, A.L.; Chen, J.J.; Hou, W.; Zhang, S.; Zhao, Y.H.; Li, X.R.; Hou, Y.H.; LAMOST MRS Collaboration. SPCANet: Stellar Parameters and Chemical Abundances Network for LAMOST-II Medium Resolution Survey. *Astrophys. J.* **2020**, *891*, 23. [CrossRef]
18. Yi, Z.; Luo, A.; Song, Y.; Zhao, J.; Shi, Z.; Wei, P.; Ren, J.; Wang, F.; Kong, X.; Li, Y.; et al. M Dwarf Catalog of the LAMOST Pilot Survey. *Astron. J.* **2014**, *147*, 33. [CrossRef]
19. Karoff, C.; Knudsen, M.F.; De Cat, P.; Bonanno, A.; Fogtmann-Schulz, A.; Fu, J.; Frasca, A.; Inceoglu, F.; Olsen, J.; Zhang, Y.; et al. Observational evidence for enhanced magnetic activity of superflare stars. *Nat. Commun.* **2016**, *7*, 11058. [CrossRef]
20. Zhang, L.; Lu, H.; Han, X.L.; Jiang, L.; Li, Z.; Zhang, Y.; Hou, Y.; Wang, Y.; Cao, Z. Chromospheric activity of periodic variable stars (including eclipsing binaries) observed in DR2 LAMOST stellar spectral survey. *New Astron.* **2018**, *61*, 36–58. [CrossRef]
21. Zhang, L.Y.; Long, L.; Shi, J.; Lu, H.P.; Gao, Q.; Han, X.L.; Wang, H.; Prabhakar, M.; Lamost Mrs Collaboration. Magnetic activity based on LAMOST medium-resolution spectra and the Kepler survey. *Mon. Not. R. Astron. Soc.* **2020**, *495*, 1252–1270. [CrossRef]
22. Frasca, A.; Molenda-Żakowicz, J.; De Cat, P.; Catanzaro, G.; Fu, J.N.; Ren, A.B.; Luo, A.L.; Shi, J.R.; Wu, Y.; Zhang, H.T. Activity indicators and stellar parameters of the Kepler targets. An application of the ROTFIT pipeline to LAMOST-Kepler stellar spectra. *Astron. Astrophys.* **2016**, *594*, A39. [CrossRef]
23. Zhang, L.Y.; Yue, Q.; Lu, H.P.; Han, X.M.L.; Zhang, Y.; Shi, J.R.; Wang, Y.F.; Hou, Y.H.; Zi-Huang, C. Radio stars observed in the LAMOST spectral survey. *Res. Astron. Astrophys.* **2017**, *17*, 105. [CrossRef]
24. Gizis, J.E.; Reid, I.N.; Hawley, S.L. The Palomar/MSU Nearby Star Spectroscopic Survey. III. Chromospheric Activity, M Dwarf Ages, and the Local Star Formation History. *Astron. J.* **2002**, *123*, 3356–3369. [CrossRef]
25. Lee, K.G.; Berger, E.; Knapp, G.R. Short-term Hα Variability in M Dwarfs. *Astrophys. J.* **2010**, *708*, 1482–1491. [CrossRef]
26. Cui, X.Q.; Zhao, Y.H.; Chu, Y.Q.; Li, G.P.; Li, Q.; Zhang, L.P.; Su, H.J.; Yao, Z.Q.; Wang, Y.N.; Xing, X.Z.; et al. The Large Sky Area Multi-Object Fiber Spectroscopic Telescope (LAMOST). *Res. Astron. Astrophys.* **2012**, *12*, 1197–1242. [CrossRef]
27. Zhao, G.; Zhao, Y.H.; Chu, Y.Q.; Jing, Y.P.; Deng, L.C. LAMOST spectral survey—An overview. *Res. Astron. Astrophys.* **2012**, *12*, 723–734. [CrossRef]
28. Li, D.; Dickey, J.M.; Liu, S. Preface: Planning the scientific applications of the Five-hundred-meter Aperture Spherical radio Telescope. *Res. Astron. Astrophys.* **2019**, *19*, 016. [CrossRef]
29. Wu, Y.; Luo, A.L.; Li, H.N.; Shi, J.R.; Prugniel, P.; Liang, Y.C.; Zhao, Y.H.; Zhang, J.N.; Bai, Z.R.; Wei, P.; et al. Automatic determination of stellar atmospheric parameters and construction of stellar spectral templates of the Guoshoujing Telescope (LAMOST). *Res. Astron. Astrophys.* **2011**, *11*, 924–946. [CrossRef]
30. Covey, K.R.; Ivezić, Ž.; Schlegel, D.; Finkbeiner, D.; Padmanabhan, N.; Lupton, R.H.; Agüeros, M.A.; Bochanski, J.J.; Hawley, S.L.; West, A.A.; et al. Stellar SEDs from 0.3 to 2.5 μm: Tracing the Stellar Locus and Searching for Color Outliers in the SDSS and 2MASS. *Astron. J.* **2007**, *134*, 2398–2417. [CrossRef]
31. West, A.A.; Morgan, D.P.; Bochanski, J.J.; Andersen, J.M.; Bell, K.J.; Kowalski, A.F.; Davenport, J.R.A.; Hawley, S.L.; Schmidt, S.J.; Bernat, D.; et al. The Sloan Digital Sky Survey Data Release 7 Spectroscopic M Dwarf Catalog. I. Data. *Astron. J.* **2011**, *141*, 97. [CrossRef]
32. Hilton, E.J.; West, A.A.; Hawley, S.L.; Kowalski, A.F. M Dwarf Flares from Time-resolved Sloan Digital Sky Survey Spectra. *Astron. J.* **2010**, *140*, 1402–1413. [CrossRef]
33. Alam, S.; Albareti, F.D.; Allende Prieto, C.; Anders, F.; Anderson, S.F.; Anderton, T.; Andrews, B.H.; Armengaud, E.; Aubourg, É.; Bailey, S.; et al. The Eleventh and Twelfth Data Releases of the Sloan Digital Sky Survey: Final Data from SDSS-III. *Astrophys. J. Suppl. Ser.* **2015**, *219*, 12. [CrossRef]
34. Hawley, S.L.; Covey, K.R.; Knapp, G.R.; Golimowski, D.A.; Fan, X.; Anderson, S.F.; Gunn, J.E.; Harris, H.C.; Ivezić, Ž.; Long, G.M.; et al. Characterization of M, L, and T Dwarfs in the Sloan Digital Sky Survey. *Astron. J.* **2002**, *123*, 3409–3427. [CrossRef]

35. Jensen, E.L.N.; Akeson, R. Misaligned protoplanetary disks in a young binary star system. *Nature* **2014**, *511*, 567–569. [CrossRef]
36. Kurosawa, R.; Harries, T.J.; Symington, N.H. On the formation of Hα line emission around classical T Tauri stars. *Mon. Not. R. Astron. Soc.* **2006**, *370*, 580–596. [CrossRef]
37. Traven, G.; Zwitter, T.; Van Eck, S.; Klutsch, A.; Bonito, R.; Lanzafame, A.C.; Alfaro, E.J.; Bayo, A.; Bragaglia, A.; Costado, M.T.; et al. The Gaia-ESO Survey: Catalogue of Hα emission stars. *Astron. Astrophys.* **2015**, *581*, A52. [CrossRef]
38. Cao, D.; Gu, S.; Ge, J.; Wang, T.; Zhou, J.; Chang, L.; Wolter, U.; Mittag, M.; Schmitt, J.H.M.M.; Perdelwitz, V. Prominence activation, optical flare, and post-flare loops on the RS Canum Venaticorum star SZ Piscium. *Mon. Not. R. Astron. Soc.* **2019**, *482*, 988–998. [CrossRef]
39. Gu, S.H.; Tan, H.S.; Shan, H.G.; Zhang, F.H. Chromospheric activity on the RS CVn-type binary UX Arietis. *Astron. Astrophys.* **2002**, *388*, 889–898. [CrossRef]
40. Cao, D.; Gu, S.; Wolter, U.; Mittag, M.; Schmitt, J.H.M.M. Further Investigation on Chromospheric and Prominence Activity of the RS Canum Venaticorum Star SZ Piscium. *Astron. J.* **2020**, *159*, 292. [CrossRef]
41. Cao, D.; Gu, S. Chromospheric activity and rotational modulation of the RS Canum Venaticorum binary V711 Tauri during 1998–2004. *Mon. Not. R. Astron. Soc.* **2015**, *449*, 1380–1390. [CrossRef]
42. Honda, S.; Notsu, Y.; Namekata, K.; Notsu, S.; Maehara, H.; Ikuta, K.; Nogami, D.; Shibata, K. Time-resolved spectroscopic observations of an M-dwarf flare star EV Lacertae during a flare. *Publ. Astron. Soc. Jpn.* **2018**, *70*, 62. [CrossRef]
43. Moura, T.; Alencar, S.H.P.; Sousa, A.P.; Alecian, E.; Lebreton, Y. Spectroscopic analysis of accretion/ejection signatures in the Herbig Ae/Be stars HD 261941 and V590 Mon. *Mon. Not. R. Astron. Soc.* **2020**, *494*, 3512–3535. [CrossRef]
44. Meng, G.; Zhang, L.Y.; Pi, Q.F.; Long, L.; Han, X.L.; Prabhakar, M. Absolute parameters and observed flares in the M-type detached eclipsing binary 2MASS J04100497+2931023. *Res. Astron. Astrophys.* **2021**, *21*, 115. [CrossRef]
45. Pi, Q.f.; Zhang, L.y.; Bi, S.l.; Han, X.L.; Lu, H.p.; Yue, Q.; Long, L.; Yan, Y. Magnetic Activity and Orbital Period Study for the Short-period RS CVn-type Eclipsing Binary DV Psc. *Astrophys. J.* **2019**, *877*, 75. [CrossRef]
46. Jiang, P.; Tang, N.Y.; Hou, L.G.; Liu, M.T.; Krčo, M.; Qian, L.; Sun, J.H.; Ching, T.C.; Liu, B.; Duan, Y.; et al. The fundamental performance of FAST with 19-beam receiver at L band. *Res. Astron. Astrophys.* **2020**, *20*, 064. [CrossRef]
47. Li, D.; Wang, P.; Qian, L.; Krco, M.; Jiang, P.; Yue, Y.; Jin, C.; Zhu, Y.; Pan, Z.; Nan, R.; et al. FAST in Space: Considerations for a Multibeam, Multipurpose Survey Using China's 500-m Aperture Spherical Radio Telescope (FAST). *IEEE Microw. Mag.* **2018**, *19*, 112–119. [CrossRef]
48. Route, M.; Wolszczan, A. The 5 GHz Arecibo Search for Radio Flares from Ultracool Dwarfs. *Astrophys. J.* **2013**, *773*, 18. [CrossRef]
49. Vedantham, H.K.; Callingham, J.R.; Shimwell, T.W.; Tasse, C.; Pope, B.J.S.; Bedell, M.; Snellen, I.; Best, P.; Hardcastle, M.J.; Haverkorn, M.; et al. Coherent radio emission from a quiescent red dwarf indicative of star-planet interaction. *Nat. Astron.* **2020**, *4*, 577–583. [CrossRef]
50. DeBoer, D.R.; Gough, R.G.; Bunton, J.D.; Cornwell, T.J.; Beresford, R.J.; Johnston, S.; Feain, I.J.; Schinckel, A.E.; Jackson, C.A.; Kesteven, M.J.; et al. Australian SKA Pathfinder: A High-Dynamic Range Wide-Field of View Survey Telescope. *IEEE Proc.* **2009**, *97*, 1507–1521. [CrossRef]
51. Forbrich, J.; Menten, K.M.; Reid, M.J. A 1.3 cm wavelength radio flare from a deeply embedded source in the Orion BN/KL region. *Astron. Astrophys.* **2008**, *477*, 267–272. [CrossRef]
52. Forbrich, J.; Reid, M.J.; Menten, K.M.; Rivilla, V.M.; Wolk, S.J.; Rau, U.; Chandler, C.J. Extreme Radio Flares and Associated X-Ray Variability from Young Stellar Objects in the Orion Nebula Cluster. *Astrophys. J.* **2017**, *844*, 109. [CrossRef]
53. West, A.A.; Hawley, S.L.; Walkowicz, L.M.; Covey, K.R.; Silvestri, N.M.; Raymond, S.N.; Harris, H.C.; Munn, J.A.; McGehee, P.M.; Ivezić, Ž.; et al. Spectroscopic Properties of Cool Stars in the Sloan Digital Sky Survey: An Analysis of Magnetic Activity and a Search for Subdwarfs. *Astron. J.* **2004**, *128*, 426–436. [CrossRef]
54. Berger, E.; Ball, S.; Becker, K.M.; Clarke, M.; Frail, D.A.; Fukuda, T.A.; Hoffman, I.M.; Mellon, R.; Momjian, E.; Murphy, N.W.; et al. Discovery of radio emission from the brown dwarf LP944-20. *Nature* **2001**, *410*, 338–340. [CrossRef] [PubMed]
55. Berger, E.; Basri, G.; Fleming, T.A.; Giampapa, M.S.; Gizis, J.E.; Liebert, J.; Martín, E.; Phan-Bao, N.; Rutledge, R.E. Simultaneous Multi-Wavelength Observations of Magnetic Activity in Ultracool Dwarfs. III. X-ray, Radio, and Hα Activity Trends in M and L dwarfs. *Astrophys. J.* **2010**, *709*, 332–341. [CrossRef]
56. Shkolnik, E.; Walker, G.A.H.; Bohlender, D.A.; Gu, P.G.; Kürster, M. Hot Jupiters and Hot Spots: The Short- and Long-Term Chromospheric Activity on Stars with Giant Planets. *Astrophys. J.* **2005**, *622*, 1075–1090. [CrossRef]